



ELSEVIER

Surface Science 322 (1995) 151–167

surface science

# Thermally activated oxidation of $\text{NH}_3$ on $\text{Pt}(111)$ : intermediate species and reaction mechanisms

W.D. Mieher<sup>\*,1</sup>, W. Ho

*Laboratory of Atomic and Solid State Physics and Materials Science Center, Cornell University, Ithaca, NY 14853-2501, USA*

Received 13 June 1994; accepted for publication 15 September 1994

## Abstract

Results of a study of the thermally activated reactions of ammonia with atomic and molecular oxygen on  $\text{Pt}(111)$  are presented. Ultrahigh vacuum, surface sensitive techniques such as temperature programmed desorption and reaction spectroscopies (TPD, TPRS), electron energy loss spectroscopy (EELS), Auger electron spectroscopy (AES), and low energy electron diffraction (LEED) were used in this study.  $\text{H}_2\text{O}$ ,  $\text{NO}$ , and  $\text{N}_2$  are produced in various amounts depending on reactant concentrations. Stable intermediate species  $\text{OH}$ ,  $\text{NH}$ , and  $\text{NH}_2$  are identified by EELS. Assignment of reaction mechanisms based on liberation of hydrogen via stepwise  $\text{N-H}$  bond cleavage by atomic oxygen and  $\text{OH}$  is made through an EELS analysis of reaction intermediates and a TPRS analysis of  $\text{NH}_3$  coverage dependences of product distributions. A forthcoming report will describe the photo-induced reaction of  $\text{NH}_3$  and  $\text{O}_2$  coadsorbed on  $\text{Pt}(111)$ .

**Keywords:** Ammonia; Electron energy loss spectroscopy; Nitrogen; Nitrogen oxides; Oxygen; Platinum; Thermal desorption spectroscopy; Water

## 1. Introduction

The oxidation of ammonia on platinum is important in industrial processes such as the synthesis of nitric acid [1] and is relevant to pollution control devices to eliminate  $\text{NO}$  and  $\text{NO}_2$  emissions. Recent articles provide overviews of  $\text{NH}_3$  adsorption and reaction on  $\text{Pt}(111)$  [2,3] and other metals [4,5]. This study, performed under ultrahigh vacuum (UHV) conditions, complements previous steady-state, high pressure studies and other UHV studies [3,6] by identifying reaction intermediates and determining reactant

concentration dependences of product distributions. Our primary motivation for undertaking this study was to provide a basis for comparison to the study of the photolytic reaction of  $\text{NH}_3$  and  $\text{O}_2$  coadsorbed on  $\text{Pt}(111)$ , referred to as  $\text{NH}_3/\text{O}_2/\text{Pt}(111)$ , the results of which are presented in a forthcoming paper [7].

Ammonia adsorption on  $\text{Pt}(111)$  has been studied previously with a variety of techniques, characterizing the electronic [ultraviolet and X-ray photoemission spectroscopies (UPS, XPS)] [8], vibrational [electron energy loss spectroscopy (EELS)] [9], and surface bonding [thermal desorption spectroscopy (TDS)] [8] properties.  $\text{NH}_3/\text{Pt}(111)$  occurs in three distinct states. The  $\text{NH}_3$  in the first layer form chemisorption bonds to the  $\text{Pt}(111)$  surface. The second layer forms hydrogen bonds to the first layer and exhibits discernibly different vibrational frequencies

<sup>\*</sup> Corresponding author.

<sup>1</sup> Present address: Division of Applied Sciences, Harvard University, 9 Oxfordstreet, Cambridge, MA 02138, USA. Fax: +1 617 496 4654; E-mail: walter\_mieher@lucifer.harvard.edu.

and desorption temperatures than the first layer.  $\text{NH}_3$  multilayers are formed at higher coverages and resemble solid ammonia.  $\text{NH}_3$  decomposition on a clean Pt(111) surface does not proceed below 600 K [10].

Oxygen can exist in two chemisorption states on Pt(111). Atomic oxygen is formed upon dosing the Pt(111) crystal with  $\text{O}_2$  at temperatures above  $\approx 150$  K. Maximum atomic oxygen coverage attainable under normal conditions by dosing with  $\text{O}_2$  is 0.25 ML [11] (monolayer (ML);  $1 \text{ ML} \equiv 1.49 \times 10^{15} \text{ cm}^{-2}$ ). Molecular oxygen remains stable on Pt(111) when dosed at temperatures below  $\approx 150$  K. Saturation molecular oxygen coverage is 0.44 ML at 100 K [12].

Previous studies of  $\text{NH}_3$  oxidation have been performed on Pt(111) surfaces, monitoring the gas-phase products. Steady state reaction studies [6] under UHV conditions with a stepped Pt(111) surface observed that excess  $\text{NH}_3$  resulted in  $\text{N}_2$  production while under excess  $\text{O}_2$  reaction conditions NO formation was preferred. A stoichiometric gas mixture of  $\text{NH}_3$  and  $\text{O}_2$  leads to preferential  $\text{N}_2$  production for crystal temperatures 500 K and lower, while at higher temperatures NO formation dominated. No other nitrogen-containing products were detected in the gas phase. It was concluded that step edges played a dominant role in the reactivity of the stepped Pt  $12(111) \times (111)$  surface.

Another study concentrated on NO production at higher temperatures (550–1100 K) and the internal state distributions of the NO [3]. It was found that there are at least two different mechanisms for the production of NO, which was observed to have a formation temperature threshold of  $\sim 550$  K. The activation energy of the “fast” mechanism was determined to be  $29 \pm 3 \text{ kcal mol}^{-1}$  and occurred under excess  $\text{O}_2$  reaction conditions. The “slow” mechanism was found to have an activation energy of  $14 \pm 3 \text{ kcal mol}^{-1}$  and was dominant when there was excess  $\text{NH}_3$ . The angular distribution of the desorbing NO exhibited  $\cos^{3/2}\theta$  behavior with respect to the surface normal. Multiphoton ionization measurements of the NO internal state distributions concluded that both the vibrational and rotational energy distributions were characterized by temperatures lower than the crystal temperature, indicating that the NO residence time after formation was sufficient to allow accommodation of the exothermic reaction energy. Again it was suggested that steps and

defects were important in the reaction.

Reaction intermediates in the oxidation of  $\text{NH}_3$  on Ag(110) have been identified with EELS [4]. The gas-phase reaction products were also monitored with a mass spectrometer in temperature programmed reaction spectroscopy (TPRS). Stable hydroxyl and  $\text{NH}_x$  ( $x = 1, 2$ ) species were observed on the surface. It was determined that the reactions depended upon N–H bond cleavage by oxygen since  $\text{NH}_3$  does not decompose on Ag(110) in the temperature range of the study and  $\text{H}_2$  desorption was not observed under any conditions. In addition, this reference [4] presents a useful review of  $\text{NH}_3$  adsorption on transition metal surfaces.

## 2. Experimental

Experiments using temperature programmed desorption spectroscopy, temperature programmed reaction spectroscopy, electron energy loss spectroscopy, Auger electron spectroscopy (AES), and low energy electron diffraction (LEED) were performed using the apparatus described previously [13,14]. Cleaning, dosing, and all measurements except EELS were performed in the upper chamber of the two-tiered UHV system. EELS studies were conducted in the lower chamber, which houses an EEL spectrometer incorporating a multi-channel detector with time-resolved data acquisition capabilities (TREEELS). When operated in the high resolution mode to acquire information on vibrational modes of surface molecular species, the resolution was typically 8 to 10 meV. The incident electron energy was  $\sim 10 \text{ eV}$  with respect to ground, uncorrected for work function differences. The specular scattering geometry was employed ( $\theta_i = \theta_s = 63^\circ$  from the surface normal). A bias of 0 to 3 V with respect to ground was applied to the crystal to minimize the need for EEL spectrometer tuning changes, otherwise required by the large work function changes induced by ammonia adsorption. EEL spectra were analyzed with a fitting program, described previously, that performs Poisson-weighted nonlinear least-squares fits for one to four Gaussian peaks and a background (which can be constant, linear, quadratic, or exponential) for a selected region of the spectrum [13].

The Pt(111) crystal was a disk  $\approx 1 \text{ cm}$  diameter

and  $\approx 2$  mm thick, cut and polished to within  $0.5^\circ$  of the (111) plane, and mounted between two 0.5 mm Ta wires spot-welded to its edges. Crystal temperature was measured using a chromel–alumel thermocouple spot-welded to the back of the crystal and regulated by a dedicated PDP 11-23 microcomputer. A PDP 11-73 microcomputer was used to control the UTI 100c quadrupole mass spectrometer (QMS) and to monitor the crystal temperature and up to eight masses during TPRS. The QMS was enclosed by a nose cone with a 2 mm orifice positioned normal to and 2 mm from the center of the crystal, ensuring that detected species came only from the sample.

Three variable leak valves and gas handling systems allowed ease of dosing. Neon for sputtering and oxygen for cleaning and dosing ( $^{18}\text{O}_2$ , Isotec 99.3%) were admitted via separate variable leak valves.  $^{18}\text{O}_2$  was used exclusively throughout this study, therefore  $\text{O}_2$  and O are used to represent  $^{18}\text{O}_2$  and  $^{18}\text{O}$  hereafter. A 4 L  $\text{O}_2$  dose (langmuir, L,  $1 \text{ L} \equiv 1.0 \times 10^{-6}$  Torr-s) was used to ensure saturation of the crystal. All dosing of  $\text{O}_2$  and  $\text{NH}_3$  was performed at 85 K.

The ammonia (Matheson, 99.99%) was dosed using a capillary array (open diameter 11.5  $\mu\text{m}$ ) at a distance of  $\approx 2$  mm through a fixed conductance with 5.0 Torr  $\text{NH}_3$  backing pressure. A Baratron pressure gauge (MKS Model 221) was used to establish the  $\text{NH}_3$  pressure in a baked, liquid nitrogen trapped, diffusion pumped, stainless steel gas handling system. During  $\text{NH}_3$  exposure the upper chamber pressure increased by  $\approx 1 \times 10^{-11}$  Torr from the nominal background pressure of  $\approx 1 \times 10^{-10}$  Torr. The capillary array doser was mounted on a translation stage and could be positioned in front of the crystal in less than five seconds to start dosing  $\text{NH}_3$ . The  $\text{NH}_3$  was allowed to flow through the capillary array (2 cm above the sample) for 120 s prior to beginning  $\text{NH}_3$  exposure to assure equilibration of the dosing system. Gas handling system pumping lines near the fixed conductance allowed for quick ( $< 2$  s) cutoff of dosing. The capillary array was then immediately moved away from the crystal to avoid spurious effects from outgassing of the high surface area of the capillary array. The reproducibility of  $\text{NH}_3$  dosing was good with this scheme, allowing studies as a function of  $\text{NH}_3$  coverage from  $\approx 0.05$  ML to multilayer  $\text{NH}_3$  coverages.  $\text{NH}_3$  exposures are given in terms of the product of the  $\text{NH}_3$  backing pressure (Torr) and the dosing time

(s) divided by 100. Since the  $\text{NH}_3$  pressure in the gas handling system is not calibrated in terms of chamber pressure, the  $\text{NH}_3$  exposure is expressed in arbitrary units. A  $\text{NH}_3$  dose of  $\sim 7.5$  units corresponds to complete filling of the  $\text{NH}_3$  first layer and some occupation of the second layer, as determined with EELS and TPRS.

### 3. Results

TPD/TPRS studies were conducted as a function of  $\text{NH}_3$  exposure for clean Pt(111), 0.25 ML O/Pt(111), and presaturated  $\text{O}_2$ /Pt(111). EELS studies were also performed as functions of both  $\text{NH}_3$  coverage and annealing temperature for various  $\text{NH}_3$  exposures on clean, atomic oxygen, and molecular oxygen covered Pt(111) surfaces.

#### 3.1. $\text{NH}_3$ /Pt(111)

##### 3.1.1. TPD of $\text{NH}_3$ from clean Pt(111)

The adsorption of  $\text{NH}_3$  on clean Pt(111) has been studied in detail previously [2,8,9,15]. Fig. 1 shows TPD spectra for increasing exposures of  $\text{NH}_3$ /Pt(111). Three molecular  $\text{NH}_3$  desorption states are observed. At low coverages,  $\text{NH}_3$  desorption is observed from the first chemisorbed layer at temperatures up to 400 K, spreading down to  $\approx 180$  K with filling of the first layer at a dose of  $\approx 5.0$  units. The second, weakly chemisorbed layer, which is hydrogen bonded to the first layer and less strongly interacting with the Pt(111) surface, exhibits a narrower desorption peak at 150 K. Multilayer  $\text{NH}_3$  forms for  $\text{NH}_3$  exposures greater than 10.0 units, which desorbs in a sharp feature at  $\approx 100$  K, and spreads down to the dosing temperature with increasing multilayer coverage. No  $\text{NH}_3$  decomposition ( $\leq 3\%$ ) is observed as determined by the absence of nitrogen (mass 28, monitored via its mass 14 fragment) desorption signal in TPD.

##### 3.1.2. EELS of $\text{NH}_3$ on clean Pt(111)

In Fig. 2 EEL spectra are shown for the clean surface and for three  $\text{NH}_3$  exposures: 2.5 units (less than half of a full first layer,  $\leq 0.12$  ML), 5.0 units (nearly complete first and some second layer spectral features), and 10.0 units  $\text{NH}_3$  (second layer). The

Table 1

Vibrational frequencies of ammonia and fragments on Pt(111)

Species	Vibrational mode	Observed (meV)	Previously reported (meV)	Reference
NH <sub>3</sub>	$\nu(\text{Pt-N})$	44	43(39)	[9]([2])
	$\rho_r(\text{NH}_3)$	86	89	[9]
	$\delta_s$	145	141	[9]
	$\delta_d$	200	198	[9]
	$\nu_s(\text{N-H})$	390	402	[9]
	$\nu_d(\text{N-H})$	417	409	[9]([2])
NH <sub>3</sub> M <sup>a</sup>	$\delta_s$	136	148(133)	[9]([2])
	$\delta_d$	175	202(200)	[9]([2])
	$\nu_s(\text{N-H})$	378	391(365)	[9]([2])
	$\nu_d(\text{N-H})$	417	412(419)	[9]([2])
NH <sub>2</sub>	$\nu(\text{Pt-N})$		62(68 <sup>b</sup> )	[5]
	$\delta(\text{NH}_2)$	200 or 220	288	[5]
	$\nu_s(\text{N-H})$	410	407	[5]
	$\nu_d(\text{N-H})$		419 <sup>b</sup>	[5]
NH	$\nu(\text{Pt-N})$		50(77 <sup>b</sup> )	[5]
	$\delta(\text{NH})$	177	157(175 <sup>b</sup> )	[5]
	$\nu(\text{N-H})$	410	402(−417 <sup>b</sup> )	[5]
N	$\nu(\text{Pt-N})$	60	61	[5]
	Nitride	98	91	[5]
	Nitride	132		[5]

<sup>a</sup> M denotes multilayer.<sup>b</sup> From Tables in Ref. [5].

first layer exhibits the previously noted [9,2] loss features:  $\rho_r(\text{NH}_3)$  at 86 meV,  $\delta_s(\text{HNNH})_3$  at 145 meV,  $\delta_d(\text{HNNH})_3$  at 200 meV,  $\nu_s(\text{NH})_3$  at 390 meV, and  $\nu_d(\text{NH})_3$  at 417 meV. (Here the subscript “3” denotes that it is NH<sub>3</sub> since assignments to NH<sub>2</sub> are made below, and *s* and *d* indicate symmetric and degenerate modes, respectively.) Table 1 summarizes the EELS results. The vibrational frequencies presented in the text refer to the spectrum being discussed. The observed frequencies vary due to coverage-dependent and coadsorbate-induced effects; thus the numbers reported in the tables may not exactly match those discussed in the text or labeled in the figures. The  $\nu(\text{Pt-NH}_3)$  mode at 44 meV appears at higher coverages (5.0 units) and becomes quite intense as second and multilayers form. Along with the appearance of another feature at 175 meV (which we assign to a multilayer  $\delta_d(\text{HNNH})_3$  mode), the  $\delta_s(\text{HNNH})_3$  mode shifts position as the first (145 meV) and sec-

ond ( $\approx 136$  meV) layer peaks superpose and blend (unresolved at this NH<sub>3</sub> exposure, shown clearly in Fig. 10). The assignment of NH<sub>3</sub> vibrational modes follows that of Sexton and Mitchell [9] with the exception of the EELS feature at 136 meV, which we assign to multilayer  $\delta_s(\text{HNNH})_3$  by comparison to solid [ $\delta_s(\text{HNNH})_3$  at 131 meV] and liquid NH<sub>3</sub> [ $\delta_s(\text{HNNH})_3$  at 128 meV] [4].

Upon annealing of a 5.0 units NH<sub>3</sub> exposure NH<sub>3</sub>/Pt(111) surface, the  $\delta_s$  loss feature shown in Fig. 3 narrows and shifts in energy, ranging from 140 to 148 meV as observed by Sexton and Mitchell [9]. Annealing of adsorbate systems was performed by ramping the crystal temperature at 2 K s<sup>−1</sup> to the desired temperature, whereupon cessation of heating quenched the system at −5 K s<sup>−1</sup>. Some NH<sub>3</sub> decomposition occurs as evidenced by loss features at 173–179  $\delta(\text{NH})_1$ , 200  $\delta(\text{NH})_2$ , and 410 meV  $\nu(\text{N-H})$  in the spectra taken after annealing to 350 and

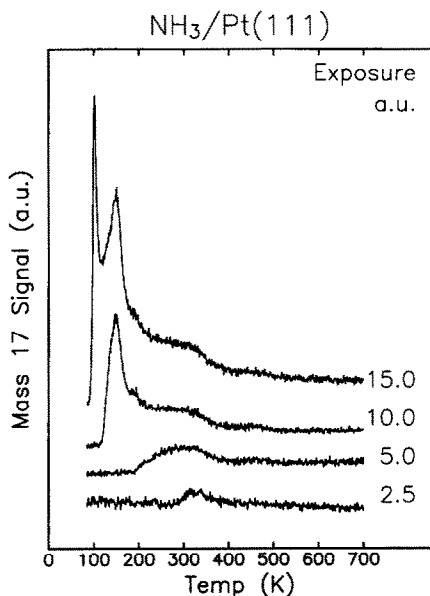


Fig. 1. TPD spectra of ammonia on Pt(111) versus exposure. At low exposures (up to 5.0 units), desorption is seen from the first layer. For higher exposures desorption is observed from the second layer at 150 K. Multilayer desorption occurs at low temperatures (starting as low as 85 K) for high  $\text{NH}_3$  exposures above 10.0–15.0 units. The crystal was dosed with ammonia using a capillary array at a distance of  $\approx 2$  mm through an uncalibrated leak with 5.0 Torr  $\text{NH}_3$  backing pressure. Exposure is determined by the product of the dosing time and the  $\text{NH}_3$  backing pressure (divided by 100) and expressed in arbitrary units. During dosing the chamber pressure increased by  $\approx 1.0 \times 10^{-11}$  from the normal background pressure of  $\approx 1.0 \times 10^{-10}$  Torr. The crystal temperature was 83–85 K for dosing and the heating rate was  $2.0 \text{ K s}^{-1}$  during TPD/TPRS experiments.

400 K. The decomposition is found by TPRS to be less than 3% of the ammonia. The assignment of  $\text{NH}_3$  fragment EELS features is made by comparison to the study by Bassignana et al. [5] of  $\text{NH}_3$  decomposition on Ni(110).

Exposure to electron beams is known [4,5,9,15,16] to dissociate  $\text{NH}_3$  on surfaces.  $\text{NH}_x$  fragments were created with a 100 eV electron beam on  $\text{NH}_3/\text{Pt}(111)$ . These fragments were then studied with EELS to facilitate EELS characterization and identification of  $\text{NH}_x$  ( $x = 1, 2$ ) fragments created during reaction of  $\text{NH}_3$  with atomic and molecular oxygen. In Fig. 3 a vibrational spectrum of a 5.0 units  $\text{NH}_3/\text{Pt}(111)$  surface after  $\approx 5 \times 10^{-3} \text{ C cm}^{-2}$ , 100 eV electron beam ex-

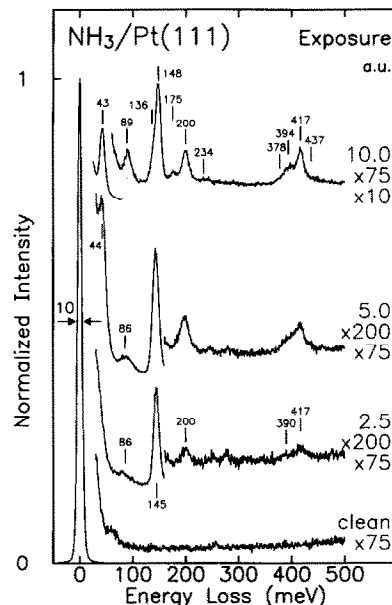


Fig. 2. EEL spectra of  $\text{NH}_3$  on Pt(111) versus exposure. Several vibrational losses are observed:  $\rho_r(\text{NH}_3)$  86 meV,  $\delta_s(\text{HNNH})_3$  145 meV,  $\delta_d(\text{HNNH})_3$  200 meV, double loss  $\delta_s(\text{HNNH})_3$  290 meV,  $\nu_s(\text{NH}_3)$  390 meV and  $\nu_d(\text{NH}_3)$  417 meV. The spectrum for 10.0 units  $\text{NH}_3$  exposure shows the appearance of an "ice" mode at 43 meV, weakening, shifting and broadening of the bright  $\text{NH}_3$  symmetric deformation at 145 meV and strengthening or appearance of other modes. The shoulder at 63 meV in the clean spectrum is a spectrometer tuning artifact. The EELS resolution was typically 8 to 10 meV for these experiments. The angles of incidence and detection were  $63^\circ$  from the surface normal.

posure reveals that there is very little ammonia left on the surface. The 177 meV  $\delta(\text{NH})$  and 410 meV  $\nu(\text{N-H})$  EELS features are well defined. The absence of  $\text{NH}_2$  features indicates that this electron beam treatment results in  $\text{NH}_2$  decomposition. A nitride feature is observed at 98 meV and atomic N at 60 meV.

### 3.2. $\text{NH}_3/\text{O}/\text{Pt}(111)$

Prior to  $\text{NH}_3$  dosing, a saturation coverage of 0.25 ML O was produced by the following procedure. An  $\text{O}_2$  pressure of  $4 \times 10^{-8}$  Torr was established and maintained for 100 s at 85 K to obtain a saturation coverage of  $\text{O}_2$  on the sample. The crystal temperature was then ramped at  $5 \text{ K s}^{-1}$  to 300 K and held for 2 min while the  $\text{O}_2$  exposure continued for 1 min before pumping out the  $\text{O}_2$ . Equilibrium on the surface

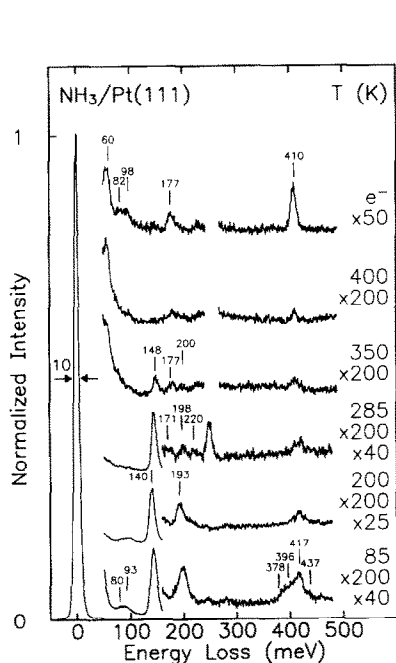


Fig. 3. EEL spectra of 5.0 units  $\text{NH}_3$  exposure on Pt(111) versus annealing temperature, except for the top spectrum which is for an electron beam exposed surface. The loss peak at 145 meV narrows and shifts upon  $\text{NH}_3$  desorption. Some  $\text{NH}_3$  thermal decomposition occurs as evidenced by loss features at 177, 200 and 410 meV in the spectra taken after annealing to 350 and 400 K. CO contamination is seen at 256 meV. The spectrum for the electron beam exposed surface ( $e^-$ ,  $\approx 5 \times 10^{-3} \text{ C cm}^{-2}$  at 100 eV) exhibits loss features at 82, 98, 177 and 410 meV indicating the presence of  $\text{NH}_x$  ( $x = 1, 2$ ) fragments.  $\text{NH}_3$  has been completely removed or decomposed since the normally intense  $\delta_s(\text{HNNH})_3$  loss at 145 meV is absent.

was established by holding the crystal temperature at 300 K for another minute in vacuum before cooling the crystal to 85 K. The total  $\text{O}_2$  exposure was  $\sim 8 \text{ L}$ .

### 3.2.1. TPRS of $\text{NH}_3/\text{O}/\text{Pt}(111)$

TPR spectra of  $\text{NH}_3/0.25 \text{ ML O}/\text{Pt}(111)$  in Fig. 4 show the production of  $\text{H}_2\text{O}$ ,  $\text{NO}$ , and  $\text{N}_2$ , along with desorption of excess  $\text{NH}_3$ . The dependence of the reaction products on  $\text{NH}_3$  exposure is shown in Fig. 5. Water desorption occurs at 350 K ( $\alpha\text{H}_2\text{O}$ ) for low  $\text{NH}_3$  coverages. A second water desorption peak grows in at 215 K ( $\beta\text{H}_2\text{O}$ ) for higher  $\text{NH}_3$  exposures.  $\text{NO}$  is produced and desorbs at 500 K at low  $\text{NH}_3$  coverages until water production reactions completely consume the oxygen at higher  $\text{NH}_3$  coverages.  $\text{N}_2$  production at 480 K grows and spreads down to 400 K as  $\text{NO}$

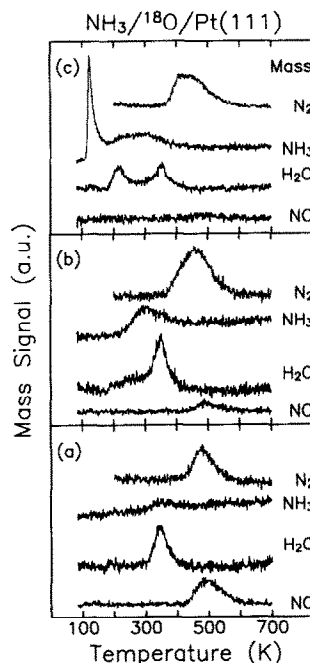


Fig. 4. TPR spectra for three ammonia exposures on 0.25 ML  $^{18}\text{O}/\text{Pt}(111)$ : (a) 2.5, (b) 5.0 and (c) 10.0 of units  $\text{NH}_3$ . The desorbing species were identified by their masses:  $\text{N}_2$  (14),  $\text{NH}_3$  (17),  $\text{H}_2^{18}\text{O}$  (20) and  $\text{N}^{18}\text{O}$  (32). The heating rate was  $2.0 \text{ K s}^{-1}$ . The magnification of frame (c) is  $\times 1/3$  compared to frames (a) and (b).

production decreases. Excess  $\text{NH}_3$  desorbs similarly to  $\text{NH}_3/\text{Pt}(111)$ .  $\text{O}_2$  recombinative desorption, which occurs at  $\sim 750 \text{ K}$  for  $\text{O}/\text{Pt}(111)$ , was not observed over the  $\text{NH}_3$  exposure range studied.  $\text{H}_2$  desorption was not observed due to water formation on the surface. Neither  $\text{N}_2\text{O}$  nor  $\text{NO}_2$  were detected.

### 3.2.2. EELS of $\text{NH}_3/\text{O}/\text{Pt}(111)$

Vibrational spectra of  $\text{O}/\text{Pt}(111)$  and for three  $\text{NH}_3$  exposures at 85 K are shown in Fig. 6. Table 2 summarizes the vibrational frequencies of the observed reaction products. The  $\text{NH}_3$  features are similar to those on the clean surface with no marked O-induced frequency shifts.  $\text{OH}$  [ $\delta(\text{OH})$  at 107 meV and  $\nu(\text{O-H})$  at 434 meV] as well as  $\text{NH}_x$  [ $x = 1, 2$  fragments (173 and 218 meV)] are formed upon  $\text{NH}_3$  exposure. The  $\delta(\text{OH})$  frequency observed is different from previous observations at 117–126 meV because of the heavier oxygen isotope (isotopic shift is  $\sim 7 \text{ meV}$ ) and the chemical environment ( $\text{O}$  and  $\text{NH}_3$ ) [17–20]. Annealing temperatures up to 285 K of 5.0 units

Table 2  
Vibrational frequencies of oxygen ( $^{18}\text{O}$ ) containing species on Pt(111)

Species	Vibrational mode	Observed (meV)	Previously reported (meV)	Reference <sup>a</sup>
$\text{O}_2$	$\nu(\text{Pt}-\text{O}_2)$		47	[12]
	$\nu_b(\text{O}-\text{O})$	82	89	[12]
	$\nu_t(\text{O}-\text{O})$	101	108	[12]
O	$\nu(\text{Pt}-\text{O})$	56	57	[12]
OH	$\delta(\text{OH})$	107–114	120–129	[17–19]
	$\nu(\text{O}-\text{H})$	433–438	424–434	[17,18]
$\text{H}_2\text{O}$	$\nu(\text{Pt}-\text{O})$		58(68)	[21]([22])
	$\rho(\text{H}_2\text{O})$		87	[19,23]
	$\delta(\text{H}_2\text{O})$	200	202	[21,22]
	$\nu_s(\text{O}-\text{H})$	435	420(422)	[21]([22])
	$\nu_d(\text{O}-\text{H})$	458	456	[21]
$\text{H}_2\text{O M}^b$	$\delta(\text{H}_2\text{O})$		205	[21]
	$\nu(\text{O}-\text{H})$		356	[21]
NO	$\nu_b(\text{Pt}-\text{N})$		38	[37]
	$\nu_t(\text{Pt}-\text{N})$		56	[37]
	$\nu_b(\text{N}-\text{O})$		184	[37]
	$\nu_t(\text{N}-\text{O})$		213	[37]

<sup>a</sup> All references are based on  $^{16}\text{O}$ .

<sup>b</sup> M denotes multilayer.

$\text{NH}_3/0.25 \text{ ML O/Pt(111)}$  produced observable concentrations of OH (107 meV) as well as N [ $\nu(\text{Pt}-\text{N})$  60 meV], NH (172–175 and 410 meV), and  $\text{NH}_2$  (196–200 and 217–223 meV) as shown in Fig. 7.  $\text{NH}_x$  fragments remained up to 380 K. Atomic N is still observed for annealing temperatures up to 650 K. Loss features at 98 and 132 meV are assigned to the nitride species, which desorbs at  $\approx 1000 \text{ K}$  [15]. The presence of  $\text{NH}_3$  vibrational modes at 200 and 380–420 meV and hydroxyl  $\nu(\text{O}-\text{H})$  at 434 meV makes it difficult to use EELS to detect the presence of  $\text{H}_2\text{O}$  [ $\delta(\text{HOH})$  200 meV and  $\nu(\text{O}-\text{H})$  368, 420–460 meV] [21–23]. Therefore, it cannot be conclusively determined from the EELS data whether  $\text{H}_2\text{O}$  is present on the surface at any point, although  $\text{H}_2\text{O}$  formed at temperatures below 200 K is expected to remain on the surface [19,21,24].

### 3.3. $\text{NH}_3/\text{O}_2/\text{Pt(111)}$

#### 3.3.1. TPRS of $\text{NH}_3/\text{O}_2/\text{Pt(111)}$

TPR spectra of  $\text{NH}_3$  on presaturated  $\text{O}_2/\text{Pt(111)}$  shown in Fig. 8 exhibit new features compared to those of  $\text{O}/\text{Pt(111)}$ . The  $\text{NH}_3$  exposure dependences of the reaction products and excess  $\text{NH}_3$  desorption are shown in Fig. 9. The stabilization of molecular oxygen by  $\text{NH}_3$  raises the  $\text{O}_2$  peak desorption temperature from 144 to 160 K, at which point the parallel channel of  $\text{O}_2$  dissociation leaves behind significantly more oxygen atoms in various intermediate states than was possible with the preadsorbed O surface. This is seen by the fact that the maximum total amount of water produced is  $1.9 \pm 0.1$  times larger for the reaction with molecular oxygen than with atomic oxygen, as determined by the integrated water desorption signal. (Note that the scale for all spectra in Fig. 8c is  $\times 1/2$  compared to Figs. 8a and 8b.) Since the saturation  $\text{O}_2$  coverage prior to  $\text{NH}_3$  dosing is 0.44 ML

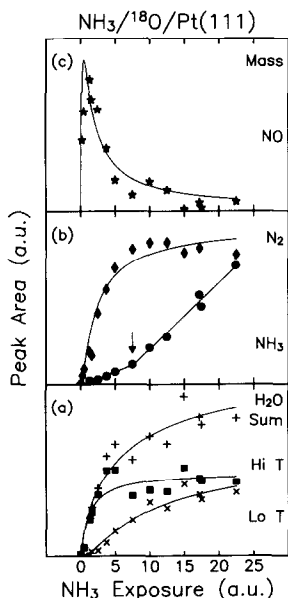


Fig. 5. The area of the TPRS peaks versus ammonia exposure for the reaction of NH<sub>3</sub> with 0.25 ML <sup>18</sup>O/Pt(111). (a) The 350 K  $\alpha$ H<sub>2</sub>O production peak area ( $\blacksquare$ , Hi T), the 215 K  $\beta$ H<sub>2</sub>O production peak area ( $\times$ , Lo T), and total H<sub>2</sub>O production ( $+$ , sum) versus NH<sub>3</sub> exposure. (b) N<sub>2</sub> production peak area ( $\blacklozenge$ ) and total NH<sub>3</sub> desorption ( $\bullet$ ). (c) NO production peak area ( $*$ ) increases at low NH<sub>3</sub> exposures until consumption of O by H<sub>2</sub>O production causes NO production to decrease. The line through the 350 K  $\alpha$ H<sub>2</sub>O data is a fit based on the Langmuir isotherm equation. This model is used to describe the concentration of N, O and 215 K  $\beta$ H<sub>2</sub>O production sites to fit the data for production of NO, N<sub>2</sub> and 215 K  $\beta$ H<sub>2</sub>O. The NH<sub>3</sub> desorption data are fit by linear functions from 0 to 7.5 units and from 7.5 to 22.5 units NH<sub>3</sub> exposure. The arrow indicates the transition point.

compared to 0.25 ML for O, up to 3.5 times more oxygen is available for reaction (prior to O<sub>2</sub> desorption), ignoring possible displacement of O<sub>2</sub> by NH<sub>3</sub> adsorption. Even though the integrated O<sub>2</sub> desorption is reduced 50% by NH<sub>3</sub> coadsorption, displacement of O<sub>2</sub> by NH<sub>3</sub> adsorption is not a factor leading to a decrease in O<sub>2</sub> desorption signals. TPRS measurements are able to account for more than 90% of the oxygen desorbing as O<sub>2</sub> and H<sub>2</sub>O, indicating that less than 10% of O<sub>2</sub> is displaced from the surface. Little change occurs in the behavior of excess NH<sub>3</sub> desorption. The slopes of the integrated peak area of NH<sub>3</sub> desorption versus exposure, above 7.5 units of NH<sub>3</sub>, are the same (within  $\pm 10\%$ ) for NH<sub>3</sub>/Pt(111), NH<sub>3</sub>/O/Pt(111),

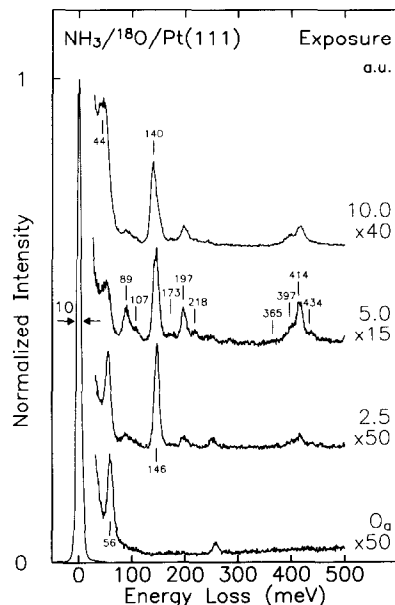


Fig. 6. EEL spectra of NH<sub>3</sub> on 0.25 ML <sup>18</sup>O/Pt(111) versus NH<sub>3</sub> exposure at 85 K. Some OH formation is indicated by the presence of loss peaks at 107 and 434 meV.

and NH<sub>3</sub>/O<sub>2</sub>/Pt(111).

In comparison with NH<sub>3</sub>/O/Pt(111), H<sub>2</sub>O production/desorption for NH<sub>3</sub>/O<sub>2</sub>/Pt(111) occurs nearly continuously from  $\approx 180$  K to 400 K at all NH<sub>3</sub> exposures, becoming enhanced at lower temperatures with increasing NH<sub>3</sub> coverage. This mix of H<sub>2</sub>O production mechanisms contrasts with the well-separated coverage dependences of the 350 K  $\alpha$ H<sub>2</sub>O and 215 K  $\beta$ H<sub>2</sub>O production peaks with O/Pt(111). At low NH<sub>3</sub> coverages, some H<sub>2</sub>O desorption signal is observed at the same temperature as O<sub>2</sub> desorption/dissociation but does not appear at higher NH<sub>3</sub> coverages. Similar H<sub>2</sub>O desorption temperatures have been reported for 1 L exposures of H<sub>2</sub>O/Pt(111) [21,24]. It is also possible that this is the result of reaction with a "hot" oxygen atom produced during O<sub>2</sub> thermal dissociation. (The term "hot" is used to describe the energetic nature of the short-lived nonequilibrium state of the atom after release from the parent molecule but before accommodation with the surface.) However, the small H<sub>2</sub>O signal ( $< 2\%$  of maximum) was not reproducible enough to correlate with O<sub>2</sub> or NH<sub>3</sub> concentrations. H<sub>2</sub> desorption was not observed, which is as expected

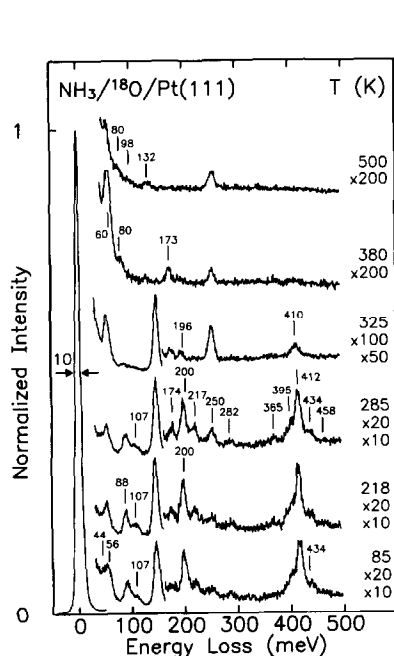


Fig. 7. EEL spectra of 5.0 units  $\text{NH}_3$  exposure on  $^{18}\text{O}/\text{Pt}(111)$  versus annealing temperature. OH (107 and 434 meV) is observed on the surface at 85 K and after annealing up to 285 K. Upon annealing to 325 K neither OH nor  $\text{H}_2\text{O}$  are observed on the surface. Some O is still present along with N, NH,  $\text{NH}_2$  and  $\text{NH}_3$ . The loss feature at 60 meV after annealing to 380 K is assigned to atomic N. Some  $\text{NH}_x$  fragments still remain (173, 200 and weak 410 meV losses), but  $\text{NH}_3$  is absent. N is still observed after annealing to 500 K. The nitride features at 98 and 132 meV disappear upon annealing to 1000 K.

in the presence of large oxygen concentrations. TPR spectra in studies of CO oxidation by coadsorbed  $\text{O}_2$  on Pt(111) exhibit a sharp  $\text{CO}_2$  desorption feature at the same temperature as  $\text{O}_2$  desorption and dissociation [25]. CO [26,27],  $\text{NH}_3$  [7], NO [28], and H [20] react with photolytically generated hot O atoms on Pt(111) at 85 K.

NO and  $\text{N}_2$  production also are different in the reaction of  $\text{NH}_3$  with  $\text{O}_2$ . Maximum NO production is about twice as much as that on the atomic oxygen surface, consistent with the availability of more oxygen and with higher  $\text{NH}_3$  exposure at maximum NO production. NO is still produced at high  $\text{NH}_3$  exposure as two NO desorption peaks at 316 and 486 K, but is again decreased sharply as oxygen is consumed by  $\text{H}_2\text{O}$  production. Maximum  $\text{N}_2$  production is 2.5 times greater, with  $\approx 0.3$  ML N on the surface. This

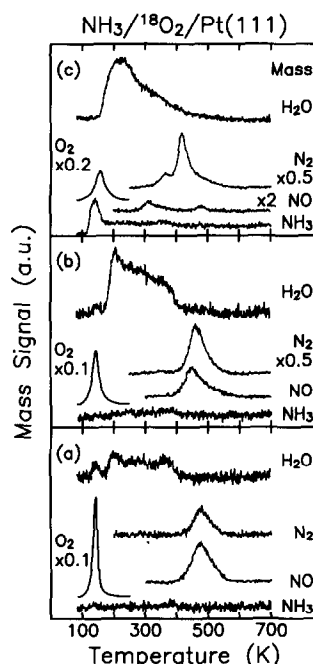


Fig. 8. TPR spectra for three  $\text{NH}_3$  exposures on  $^{18}\text{O}_2$  precov. Pt(111) surface: (a) 2.5, (b) 5.0 and (c) 10.0 units  $\text{NH}_3$ . The desorbing species were identified by their masses:  $\text{N}_2$  (14),  $\text{NH}_3$  (17),  $\text{H}_2^{18}\text{O}$  (20),  $\text{N}^{18}\text{O}$  (32), and  $^{18}\text{O}_2$  (36). The heating rate was  $2.0 \text{ K s}^{-1}$ . The scale for all spectra in frame (c) is  $\times 1/2$  compared to the frames (a) and (b).

agrees with the fact that the maximum atomic N concentration on the surface prepared with O is limited to  $\approx 0.17$  ML (0.13 ML in practice) by the amount of O available to remove H from  $\text{NH}_3$ . At high  $\text{NH}_3$  exposures the major  $\text{N}_2$  desorption occurs at 420 K and a second  $\text{N}_2$  production peak appears at 360 K. This is due to excess N on the surface. Recombinative  $\text{O}_2$  desorption occurs at  $\approx 750$  K for low  $\text{NH}_3$  exposures ( $\leq 2.5$  units).

AES studies of a surface prepared by annealing 10.0 units  $\text{NH}_3/\text{O}_2/\text{Pt}(111)$  to 380 K yield an Auger peak ratio,  $[\text{Pt}(390) + \text{N}(390)]/\text{Pt}(238)$ , of  $0.59 \pm 0.03$ . LEED observations of this surface showed a  $(2 \times 2)$  pattern identical to that for a 0.25 ML O/Pt(111) surface. The same Auger peak ratio measurements for 0.25 ML NO/Pt(111) yield a ratio of  $0.59 \pm 0.02$ . The NO was prepared by saturating clean Pt(111) with NO and then annealing to 250 K. From the AES and LEED data we determine that the atomic N coverage for the described surface is 0.25 ML and all other N and  $\text{NH}_3$  coverages are based on this calibration. This

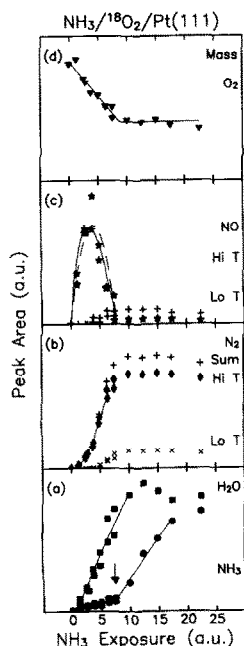


Fig. 9. The areas of the TPRS peaks versus  $\text{NH}_3$  exposure for the reaction of  $\text{NH}_3$  with  $^{18}\text{O}_2/\text{Pt}(111)$  (initial  $\text{O}_2$  coverage prior to  $\text{NH}_3$  exposure is 0.44 ML). (a) Total  $\text{H}_2\text{O}$  production ( $\blacksquare$ ) and  $\text{NH}_3$  desorption ( $\bullet$ ). (b) The main (420 to 480 K)  $\text{N}_2$  production peak ( $\blacklozenge$ , Hi T), the second (360 K)  $\text{N}_2$  production peak ( $\times$ , Lo T) and total  $\text{N}_2$  production ( $+$ , sum). (c) The main NO (450 K) production peak area ( $*$ , Hi T) and the second (315 K) NO production peak ( $+$ , Lo T). (d)  $\text{O}_2$  molecular desorption at  $\approx 150$  K. The  $\text{O}_2$  peak desorption temperature shifts up from 144 K (no  $\text{NH}_3$ ) to 160 K (22.5 units) with  $\text{NH}_3$  exposure. The straight line through the  $\text{H}_2\text{O}$  production data (a) below 10.0 units  $\text{NH}_3$  exposure describes the  $\text{H}_2\text{O}$  data better than the Langmuir isotherm model. This linear dependence is used to describe the concentration of N and O to fit the data for production of  $\text{N}_2$  (Hi T) and NO (Hi T) for  $\text{NH}_3$  exposures below 6.25 and 7.5 units respectively. The  $\text{NH}_3$  and  $\text{O}_2$  desorption data are fit by straight lines above and below the break point (indicated by the arrow) of 7.5 units  $\text{NH}_3$  exposure. The slopes of the  $\text{NH}_3$  desorption data versus exposure above 7.5 units are the same ( $\pm 10\%$ ) for  $\text{NH}_3/\text{Pt}(111)$ ,  $\text{NH}_3/\text{O}/\text{Pt}(111)$  and  $\text{NH}_3/\text{O}_2/\text{Pt}(111)$ . The exposure dependences of the reaction product peak areas for  $\text{NH}_3/\text{O}_2/\text{Pt}(111)$  are similar to but qualitatively different from those of  $\text{NH}_3/\text{O}/\text{Pt}(111)$ .

result agrees with previous work [15].

### 3.3.2. EELS of $\text{NH}_3/\text{O}_2/\text{Pt}(111)$

Molecular oxygen exhibits two stretching frequencies on  $\text{Pt}(111)$ :  $\nu(\text{O}-\text{O})$  101 meV assigned to  $^{18}\text{O}_2$  in the atop site and 82 meV for bridge-bonded  $^{18}\text{O}_2$ , as seen in Fig. 10 [11]. OH or  $\text{H}_2\text{O}$  forma-

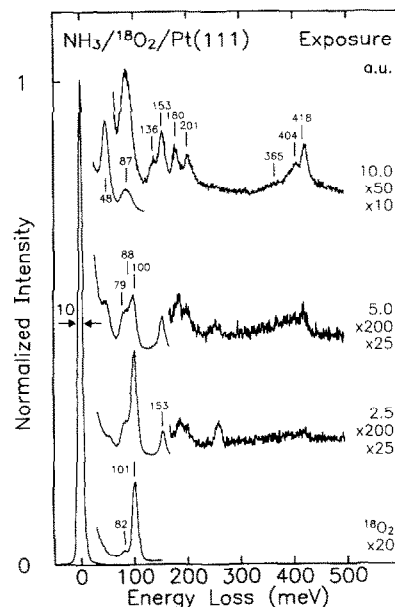


Fig. 10. EEL spectra of 0.44 ML  $^{18}\text{O}_2/\text{Pt}(111)$  followed by various exposures of  $\text{NH}_3$  at 85 K. Neither OH nor  $\text{H}_2\text{O}$  are formed upon dosing at 85 K.  $\delta_s(\text{HNNH})_3$  appears at 153 meV, shifted from the frequency observed on clean surface by the presence of  $\text{O}_2$ . The vibrational features due to multilayer  $\text{NH}_3$  (136, 180 and 365 meV) are more intense than for the same  $\text{NH}_3$  exposure on clean  $\text{Pt}(111)$ .

tion upon  $\text{NH}_3$  adsorption on  $\text{O}_2/\text{Pt}(111)$  at 85 K is much less than on  $\text{O}/\text{Pt}(111)$  based on the absence of  $\nu(\text{O}-\text{H})$  at 434 meV and  $\delta(\text{OH})$  at 110 meV. The 101 meV  $\text{O}_2$  loss peak decreases in intensity rapidly as  $\text{NH}_3$  is added to the surface, leaving a broad loss peak centered at  $\sim 87$  meV, which contains the unresolved 82 meV  $\text{O}_2$  mode, 86 meV  $\rho_f(\text{NH}_3)$  at 86 meV and perhaps perturbed or unresolved atop  $\text{O}_2$  losses as well. The 153 meV  $\delta_s(\text{HNNH})_3$  initially increases in intensity as  $\text{NH}_3$  is added to the surface. Its intensity then decreases as second or multilayers of  $\text{NH}_3$  are formed, as shown by the strong  $\delta_s(\text{HNNH})_3$  loss feature at 136 meV. The 48 meV ice mode, and 136, 180, and 365 meV loss features become more intense for higher  $\text{NH}_3$  exposures.

Heating the surface to 156 K (Fig. 11) produces copious amounts of OH [ $\delta(\text{OH})$  at 110 meV,  $\nu(\text{O}-\text{H})$  at 437 meV], as well as O [ $\nu(\text{Pt}-\text{O})$  at 56 meV], N [ $\nu(\text{Pt}-\text{N})$  at 60 meV], and  $\text{NH}_x$  fragments.  $\text{NH}_3$  and some bridge  $\text{O}_2$  are still present after heating to

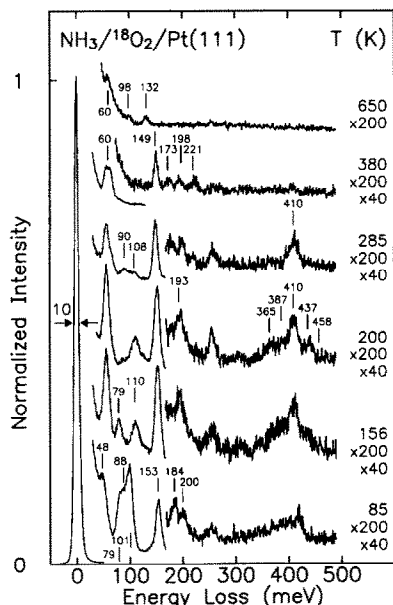


Fig. 11. EEL spectra versus annealing temperature of 0.44 ML  $^{18}\text{O}_2/\text{Pt}(111)$  followed by 5.0 units  $\text{NH}_3$  at 85 K. Substantial OH (110 and 437 meV) concentrations are observed on the surface after annealing to 156 and 200 K. After annealing to 285 K most of the OH has been consumed. N (60 meV), NH and  $\text{NH}_2$  fragments (173, 198, 221 and 410 meV) are observed for 285 and 380 K annealing temperatures. Some nitrogen and nitride species remain to 650 K as seen by loss features at 60, 98, 132 meV.

156 K. Other complexes may also exist. The surface vibrational spectrum is largely unchanged upon annealing to 200 K with the exception that  $\text{O}_2$  is no longer present on the surface. OH is still observed after annealing up to 285 K. As noted above, the vibrational modes of OH and  $\text{NH}_3$  make EELS detection of  $\text{H}_2\text{O}$  on the surface difficult at this resolution, although  $\text{H}_2\text{O}$  desorption is observed in TPRS over this same temperature range. Most of the  $\text{NH}_3$  desorption and water production are completed upon annealing to 380 K, with mostly N (60 meV), NH (173 and 410 meV),  $\text{NH}_2$  (200 and 217–223, 410 meV), and  $\text{NH}_3$  (149 meV) remaining with some O. Atomic N and nitride species (98 and 132 meV) are still detectable after annealing to 650 K but are not present in EELS after annealing to 1050 K.

## 4. Modeling

### 4.1. TPRS of $\text{NH}_3/\text{O}/\text{Pt}(111)$

The TPRS product yield data in Fig. 5 are modeled well with functions (based on the Langmuir adsorption isotherm equation) describing  $\text{NH}_3$  adsorption in sites that are active for  $\alpha\text{H}_2\text{O}$  production,

$$\theta_{\alpha\text{H}_2\text{O}} = \frac{Akx}{1 + kx}, \quad (1)$$

where  $x$  is the  $\text{NH}_3$  exposure,  $k$  scales the coverage dependence, and  $A$  scales the magnitude of the  $\alpha\text{H}_2\text{O}$  desorption signal, the water produced in the 350 K desorption peak. The initial 0.25 ML oxygen coverage contributes a constant factor to  $A$  in both Eqs. (1) and (2). The coverage dependences were fit separately for all the products by independently scaling  $A$  and  $k$  in each data set. The 215 K water production dependence was fit under the assumption that  $\beta\text{H}_2\text{O}$  is produced only after available  $\alpha\text{H}_2\text{O}$  production sites are occupied.

$$\theta_{\beta\text{H}_2\text{O}} = A \left( \frac{kx}{1 + kx} \right)^2. \quad (2)$$

Here one factor of  $\frac{kx}{1 + kx}$  describes the total hydrogen concentration on the surface and the other expresses the occupation of  $\alpha\text{H}_2\text{O}$  sites, which activate neighboring  $\beta\text{H}_2\text{O}$  sites. The main feature of this power dependence is the delayed onset of  $\beta\text{H}_2\text{O}$  production compared to  $\alpha\text{H}_2\text{O}$ .

Similar treatments provide an understanding of the data for NO and  $\text{N}_2$  production. Again, the nitrogen concentration is expressed as  $\frac{kx}{1 + kx}$  while the atomic oxygen availability is  $1 - \theta_{\alpha\text{H}_2\text{O}}$ . The NO production is given by

$$\theta_{\text{NO}} = \frac{Akx}{(1 + kx)^2}. \quad (3)$$

This function reproduces the increase and decrease of the NO production. The behavior of the  $\text{N}_2$  reaction is reproduced by

$$\theta_{\text{N}_2} = A \left( \frac{kx}{1 + kx} \right)^2. \quad (4)$$

The ammonia desorption data was fit with separate linear functions for data below and above the onset of second layer  $\text{NH}_3$  desorption.

#### 4.2. TPRS of $\text{NH}_3/\text{O}_2/\text{Pt}(111)$

$\text{H}_2\text{O}$  production from  $\text{NH}_3/\text{O}_2/\text{Pt}(111)$ , does not proceed in easily separated reaction steps, but instead occurs over a large temperature range via presumed multiple mechanisms at all coverages. It is therefore necessary to apply modeling to the coverage dependences of the product distributions different than that applied to  $\text{NH}_3/\text{O}/\text{Pt}(111)$ . The observation, especially at higher  $\text{NH}_3$  exposures, that some NO and  $\text{N}_2$  production occur at lower temperatures before  $\text{H}_2\text{O}$  production is completed, complicates the task of fitting to obtain qualitative understanding of the data. Qualitative agreement with all the data can be obtained over a limited coverage range by functions based on an empirical description of the  $\text{H}_2\text{O}$  production data. The  $\text{H}_2\text{O}$  formation reaction determines the concentration of oxygen and nitrogen available for other reactions. Applying a linear fit to the total  $\text{H}_2\text{O}$  production data in Fig. 9 for  $\text{NH}_3$  exposures below 7.5 units (where  $\text{NH}_3$  and  $\text{O}_2$  desorption exhibit sharp changes in their  $\text{NH}_3$  exposure dependences) produces reasonable agreement with the  $\text{H}_2\text{O}$  desorption data. This result can be understood if  $\text{NH}_3$  has a constant sticking coefficient ( $\sim 1$  in the case of  $\text{NH}_3$ ) and if the  $\text{H}_2\text{O}$  formation probability is also constant over this exposure range. For submonolayer coverages on the clean surface, and in the multilayer region on clean, O, and  $\text{O}_2$  covered surfaces, a constant sticking coefficient for  $\text{NH}_3$  is observed, supporting a constant  $\text{NH}_3$  sticking coefficient for lower  $\text{NH}_3$  coverages on oxygen pre-covered surfaces as well.

The oxygen concentration is determined by the amount of oxygen consumed, whereas the nitrogen concentration is determined by the amount made available by  $\text{NH}_3$  decomposition during water formation. Therefore a linear function is used to describe the concentration of oxygen. Two different functional forms are proposed for modeling the  $\text{NH}_3$  coverage dependence for NO and  $\text{N}_2$  production. The first is the same as that used for  $\text{NH}_3/0.25 \text{ ML O}/\text{Pt}(111)$  and yields the same equation as Eq. (4) for  $\text{N}_2$  production and Eq. (5) for NO production.

$$\theta_{\text{NO}} = A \frac{kx}{1 + kx} (1 - x/x_0), \quad (5)$$

The fit to Eq. 5 is shown by the solid line in Fig. 9c. The second model (dashed line in Fig. 9c) uses a

purely linear form (instead of the Langmuir adsorption isotherm form used previously) to describe the reactive nitrogen concentration,

$$\theta_{\text{NO}} = Akx(1 - x/x_0). \quad (6)$$

where  $x_0$  is an empirical parameter expressing the cut-off of NO production (due to lack of oxygen availability), in agreement with the “knee” of the coverage dependences of  $\text{O}_2$  and  $\text{NH}_3$  desorption on  $\text{NH}_3$  exposure. These two functions give similar agreement with the data over the selected exposure range.

### 5. Discussion

It is difficult to unambiguously determine the reaction mechanisms for a system that has four observed reaction products, many with multiple desorption features, formed from a veritable plethora of intermediate species. With high reactant concentrations, the electron accepting nature of  $\text{O}_2$ , and the electron donation properties of  $\text{NH}_3$ , complex formation becomes a real possibility although EELS data gave no indication of this occurring. In view of these challenges, a model is proposed. The key points are set out from the start: (1) oxygen atoms are the agents responsible for activating N–H bond cleavage; (2) all hydrogen from reacting ammonia molecules eventually form water, not  $\text{H}_2$  nor recombinative  $\text{NH}_3$ ; (3) oxygen generally will react preferentially with hydrogen rather than nitrogen except in the case of very high nitrogen concentrations ( $\geq 0.25 \text{ ML}$ ), where coverage-dependent effects become important.

The discussion proceeds as follows: First the adsorption of  $\text{NH}_3$  on  $\text{Pt}(111)$  and the effects of preadsorbed O or  $\text{O}_2$  are summarized. Then the effects of  $\text{NH}_3$  coadsorption on  $\text{O}_2$  adsorption are discussed. Next, the reactions and mechanisms for water formation are examined. Finally the  $\text{N}_2$  and NO formation reactions and mechanisms are considered.

#### 5.1. Ammonia

Excess ammonia desorption is not fundamentally changed by the presence of oxygen on  $\text{Pt}(111)$ . Although oxygen is available for reaction, approximately 30% of first layer  $\text{NH}_3$  desorbs from  $\text{O}/\text{Pt}(111)$ ,

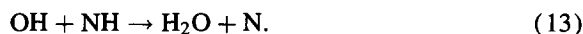
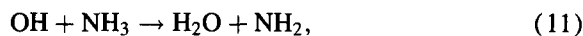
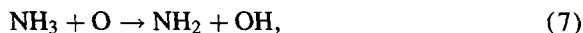
[20% from O<sub>2</sub>/Pt(111)], as determined by comparison of the slopes of the coverage dependences of NH<sub>3</sub> desorption above and below the “knee” at 7.5 units NH<sub>3</sub> exposure. The slopes of the NH<sub>3</sub> desorption data vs NH<sub>3</sub> exposure are the same within 10% for exposures greater than 7.5 units, indicating that NH<sub>3</sub> adsorption in second and multilayer states is not strongly affected by oxygen. From the Auger and LEED calibration of atomic N coverage, and from the comparison of NH<sub>3</sub> desorption from the different surfaces, the first layer coverage of ammonia is found to be 0.25 ML.

## 5.2. Molecular oxygen

Molecular oxygen is stabilized on the Pt(111) surface by ammonia, similarly to Ag(110) [4]. The O<sub>2</sub> peak desorption temperature remains nearly constant at 144 ± 1 K for NH<sub>3</sub> exposures up to 5.0 units, then rises sharply to ≈ 155 K over the range from 5.0 to 10.0 units, until reaching a maximum of 160 K at 17.5 units NH<sub>3</sub> exposure. Approximately twice as much water is formed in the reaction of 10.0 units NH<sub>3</sub> with presaturated O<sub>2</sub> than with 0.25 ML O on Pt(111). As the surface is heated above ≈ 150 K where O<sub>2</sub> desorption competes with dissociation, the presence of NH<sub>3</sub> allows more oxygen to remain on the surface in various intermediate states than on clean Pt(111).

## 5.3. Water formation reactions

The possible reaction steps in water formation are given below.

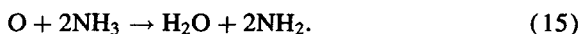


### 5.3.1. NH<sub>3</sub>/O/Pt(111)

The maximum total water production is limited to 0.25 ML H<sub>2</sub>O by the initial O concentration, ignoring NO production, which is negligible at high NH<sub>3</sub> coverages. The fact that OH is observed in EEL spectra of 2.5 units NH<sub>3</sub>/O/Pt(111) for which H<sub>2</sub>O desorption occurs only at 350 K, suggests that αH<sub>2</sub>O production involves OH which may be formed at temperatures lower than 300–350 K reaction (7). Therefore the limiting step for H<sub>2</sub>O production is reaction (12) or (13). reaction (11) can be ruled out as the primary mechanism for H<sub>2</sub>O production (especially αH<sub>2</sub>O) since the maximum concentration of N containing species participating in the reaction with 0.25 ML O is ≈ 0.13 ML (determined from the N<sub>2</sub> TPRS data). This result is close to the maximum  $\frac{2}{3} \times 0.25 = 0.17$  ML expected if all hydrogen from reacted ammonia forms water (NO formation is negligible at high NH<sub>3</sub> coverages and occurs at higher temperatures than water formation), i.e.,



If (11) dominated over (12) and (13), 0.5 ML N would remain on the surface as NH<sub>2</sub> species,



The observation of NH and NH<sub>2</sub> on the surface at higher temperatures than NH<sub>3</sub> indicates that the fragments are stable. N–H bond cleavage becomes progressively more difficult as H atoms are removed [3–5]. The NH<sub>3</sub>, NH<sub>2</sub>, and NH fragments involved in the 350 K H<sub>2</sub>O production peak must reside in sites where they are protected from bond cleavage activity by O or OH until 300 K. Free hydrogen must also be absent in this coverage range or water would be formed at lower temperatures. Substantial NH<sub>3</sub> is still present at 300 K, indicating that reaction (7) does not proceed to completion at lower temperatures.

NH<sub>3</sub> exposures above 2.5 units begin to produce βH<sub>2</sub>O at 215 K as well as H<sub>2</sub>O between 215 and 350 K. Desorption of βH<sub>2</sub>O starts as low as 180 K. This strong coverage-dependent effect may be due to crowding, which does not allow all NH<sub>3</sub> to be shielded from the effects of bond cleavage by oxygen. Crowding effects have been shown to be central in the production of formate from CO and OH on Rh(100) [29]. NH<sub>2</sub> and NH are bound more strongly to the surface than NH<sub>3</sub>

and are probably less mobile on the surface. This suggests that once an ammonia molecule interacts with an oxygen atom the resulting OH readily consumes another H atom as in reaction (12). Again, if reaction (11) was dominant, more N would be present on the surface than is observed, or  $\text{NH}_3$  recombination reactions would be expected to occur (which is also not observed).

Previous studies of water formation from O/Pt(111) and adsorbed (a) or gas (g) phase [19,30,31,24] hydrogen or O/Pt(111) and coadsorbed  $\text{H}_2\text{O}$  [24,17,18] have not resulted in a consensus as to the dominant water formation mechanism. In addition to reaction (10), other proposals exist:



In this study, reactions (17), (18) and (20) are not operative. If hydrogen abstraction from nitrogen species occurs only at short range (no free  $\text{H}^{\text{a}}$ ), reactions (16) and (19) can be eliminated for ammonia oxidation. The remaining choice is between  $\text{OH} + \text{OH}$  (10) or  $\text{OH} + \text{NH}_x$  reaction (11)–(13). It is concluded that reaction (10) is not the only operative mechanism since OH is detected on the surface by EELS for all  $\text{NH}_3$  coverages at temperatures much lower than  $\alpha\text{H}_2\text{O}$  production, or a strong coverage dependent effect exists for reaction (10). Since the activation energy for reaction (10) has been reported as  $4 \text{ kcal mol}^{-1}$  for water formation from O/Pt(111) and hydrogen [19],  $\alpha\text{H}_2\text{O}$  formation via reaction (10) would not be limited by the hydroxyl disproportionation reaction barrier. The data do not distinctly favor either mechanism alone. It is likely that both types of mechanisms operate over the wide coverage and temperature ranges studied.

### 5.3.2. $\text{NH}_3/\text{O}_2/\text{Pt}(111)$

Twice as much water can be produced by reaction of  $\text{NH}_3$  and  $\text{O}_2$  as with  $\text{NH}_3$  and O on Pt(111). For even the lowest  $\text{NH}_3$  exposures studied, water desorption occurs over a large temperature range from 180 to 380 K. Three  $\text{H}_2\text{O}$  desorption peaks at  $\approx 200$ ,  $\approx 280$ , and  $\approx 360$  K are discernable. The observation in EELS of copious amounts of OH for annealing temperatures from 156 to 285 K indicates that OH is an important intermediate species in the low temperature reactions. At high  $\text{NH}_3$  coverages, the low temperature (starting as low as 160 K) production of  $\text{H}_2\text{O}$  is several times stronger than the higher temperature TPRS peaks and both TPRS  $\text{H}_2\text{O}$  peaks seen from  $\text{NH}_3/\text{O}/\text{Pt}(111)$ . The high oxygen concentration on the surface after  $\text{O}_2$  dissociation forces the proximity of  $\text{NH}_3$  or  $\text{NH}_2$  to O, facilitating N–H bond cleavage activity of O atoms.

Thermal [25], electron [32], and photon [20,26–28] beam induced reactions driven by creation of hot oxygen atoms by  $\text{O}_2$  dissociation have been reported recently. Reactions involving photochemically produced hot H atoms have also been observed [33–35] but are not operative in the photoreactions of  $\text{NH}_3/\text{O}_2/\text{Pt}(111)$  since  $\text{NH}_3$  does not photodissociate in the wavelength range studied [7]. The reactions of  $\text{O}^*$ , the hot oxygen atoms created by thermal dissociation of  $\text{O}_2$  at low temperatures (160 K) must be considered.



The  $\text{O}^*$  may be able to abstract H from  $\text{NH}_3$ ,  $\text{NH}_2$  or NH as in reactions (21), (22) and (23). Reactions involving energetic hydroxyl species may also be involved. After formation in the gas phase, OH has been observed in high vibrational states up to  $v = 9$  [36]. The reactions of  $\text{NH}_3$  with  $\text{O}^*$  created by photodissociation of  $\text{O}_2$  at 85 K are discussed in a forthcoming paper [7].

### 5.4. $\text{N}_2$ and NO formation

The overall reaction for a stoichiometric mix of  $\text{NH}_3$  and O, where  $\text{N}_2$  production is small (see Fig. 5), is



From reaction (24) we can calculate the maximum amount of NO formed and the  $\text{NH}_3$  coverage at which this occurs. If we start with 0.25 ML O/Pt(111), the maximum amount of NO produced is  $\frac{2}{5} \times 0.25 = 0.10$  ML NO. This maximum should occur at 0.10 ML  $\text{NH}_3$  coverage or  $\sim 1.0$  units  $\text{NH}_3$  exposure, in good agreement with the data. The reaction with  $\text{O}_2$  results in a peak yield of about two times more NO production than for O/Pt(111) at  $\text{NH}_3$  exposure of 3.75 units. The higher exposure required arises from the greater amount of water formed due to more oxygen on the surface and the higher fraction of  $\text{NH}_3$  that desorbs instead of reacting on  $\text{O}_2$ /Pt(111).

NO formation can occur as follows:



The second mechanism (26) seems unlikely due to the fact that water formation is the dominant reaction at all coverages. NO can be formed only if there is oxygen left over after the water reactions are completed for  $\text{NH}_3$ /O/Pt(111). However, NO formation competes with  $\text{H}_2\text{O}$  formation in the reaction of  $\text{NH}_3$ /O<sub>2</sub>/Pt(111) at high  $\text{NH}_3$  concentrations. In this case, the overabundance of N-containing species ( $\geq 0.25$  ML) creates a coverage-dependent effect that favors NO formation. We conclude that reaction (26) is not the primary reaction although NH species are present at this temperature.  $\text{O}_2$  recombination occurs at higher temperatures,  $\approx 750$  K, compared to NO and  $\text{N}_2$  formation at  $\approx 500$  K. This indicates that O is not the mobile species.

Asscher et al. [3] observed a threshold temperature of 550 K for NO formation, similar to the 600 K threshold for  $\text{NH}_3$  decomposition on clean Pt(111) [10]. (In contrast, our TPRS results show NO production starting as low as 300 K and reaction completed by 600 K.) On this basis Asscher et al. concluded that under the high-temperature, molecular beam dosed, transient conditions of their experiments, direct interaction of  $\text{NH}_3$  with O was not important in the formation of NO. Instead they assert that NO formation relies on the Pt-activated decomposition of  $\text{NH}_3$  to form NH and N fragments for reactions (34) and (26),

which they assign to their “slow” and “fast” reactions, respectively. We propose that (26) may be involved under the conditions reported here for reactions involving excess  $\text{NH}_3$ , in contrast to the observation by Asscher et al. that it dominates for excess oxygen conditions. The different temperature and coverage ranges studied do not permit direct comparison with the results of Asscher et al.

Direct detection of NO on the surface during the oxidation of  $\text{NH}_3$  on Pt(111) is problematic. The  $\nu(\text{N}-\text{O})$  vibrations at 185 and 212 meV would be difficult to observe with EELS [37] because the  $\text{NH}_3$  and NH losses are at nearly the same energies. Low coverages of NO desorb [38] at 375 K on the clean surface and O is known [39] to decrease the activation energy for NO desorption. Other reports have described NO/ $\text{NH}_3$  complex formation on Pt(111) [38,40], which also results in lowered (355 K) NO desorption temperatures. NO/ $\text{NH}_3$  complex formation cannot account for either the 316 or 486 K NO desorption features. It is concluded that NO desorbs shortly following formation after complete accommodation with the surface as found by Asscher et al. [3]

A dose of 10.0 units  $\text{NH}_3$  on  $\text{O}_2$ /Pt(111) yields  $\sim 0.2$  equivalent monolayers of  $\text{N}_2$ ,  $\sim 2.5$  as much as the maximum for O/Pt(111). The maximum amount of N expected to be produced from higher coverages of  $\text{NH}_3$ /O/Pt(111) can be calculated from reaction (14):  $\frac{2}{3} \times 0.25 = 0.17$ . This in turn can yield a maximum of 0.083 ML  $\text{N}_2$  at higher coverages where NO formation is negligible. Similar processes involving adsorbed N and NH contribute to  $\text{N}_2$  production, and again the main difference between the mechanisms is H abstraction.

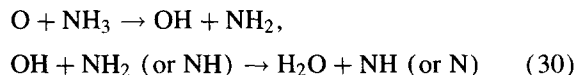


The dominant mechanism for  $\text{N}_2$  formation is reaction (27). As with NO formation via reaction (26),  $\text{N}_2$  production via reaction (28) may be involved at high  $\text{NH}_3$  exposures, although no evidence for free H<sup>a</sup> is seen.  $\text{N}_2$  production increases as the availability of O for NO formation decreases. Given the fact that  $\text{N}_2$  does not stick on Pt(111) at temperatures above

100 K, N<sub>2</sub> is not expected to reside on the surface after formation.

## 6. Summary

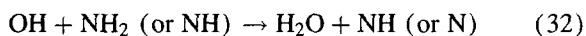
The oxidation of ammonia with atomic or molecular oxygen yields H<sub>2</sub>O, NO, and N<sub>2</sub> in varying amounts, depending on reactant concentrations. Atomic oxygen activates N–H bond cleavage, which proceeds in the order of difficulty, with NH<sub>3</sub> being the easiest followed by NH<sub>2</sub> and NH. Steps and defects do not play a major role in the reactions under the conditions studied. There is no evidence in this study to suggest that free H atoms occur at any time on the platinum surface nor are any recombinative reactions producing NH<sub>3</sub> observed. OH, NH, and NH<sub>2</sub> are directly observed with EELS and are found to be stable reaction intermediates. H<sub>2</sub>O desorption occurs over a wide temperature range from 160 to 360 K with three discernable H<sub>2</sub>O desorption features. The mechanism for low temperature H<sub>2</sub>O production is



or



At higher temperatures H<sub>2</sub>O production proceeds via



or



The stabilization of O<sub>2</sub> by NH<sub>3</sub> results in twice as much O remaining on the surface, yielding twice as much H<sub>2</sub>O over a wide temperature range. The hot O\* atoms created by O<sub>2</sub> dissociation are reactive and important in the initial creation of OH species at low temperatures. Conditions of excess oxygen yield more NO than N<sub>2</sub>. The N atoms are found to be the mobile species for NO and N<sub>2</sub> formation. The main NO production mechanism is



instead of



N<sub>2</sub> formation occurs primarily via



The determination of the reaction mechanisms is supported by direct identification of reaction intermediates and analyses of the reaction products as a function of NH<sub>3</sub> concentration.

## Acknowledgements

Support of this work by the National Science Foundation Grant No. DMR-9015823 is gratefully acknowledged. We thank Marcus Weldon for critical reading of the manuscript.

## References

- [1] T.H. Chilton, The Manufacture of Nitric Acid by the Oxidation of Ammonia, Chemical Engineering Progress Monograph Series, No. 3, Vol. 56 (American Institute of Chemical Engineers, New York, 1960).
- [2] J.M. Gohndrone, C.W. Olsen, A.L. Backman, T.R. Gow, E. Yagasaki and R.I. Masel, J. Vac. Sci. Technol. A 7 (1989) 1986.
- [3] M. Asscher, W.L. Guthrie, T.-H. Lin and G.A. Somorjai, J. Phys. Chem. 88 (1984) 3233.
- [4] D.M. Thornburg and R.J. Madix, Surf. Sci. 220 (1989) 268.
- [5] I.C. Bassignana, K. Wagemann, J. Küppers and G. Ertl, Surf. Sci. 175 (1986) 22.
- [6] J.L. Gland and V.N. Korchak, J. Catal. 53 (1978) 9.
- [7] W.D. Mieher and W. Ho, to be published.
- [8] G.B. Fisher, Chem. Phys. Lett. 79 (1981) 452.
- [9] B.A. Sexton and G.E. Mitchell, Surf. Sci. 99 (1980) 523, 539.
- [10] W.L. Guthrie, J.D. Sokol and G.A. Somorjai, Surf. Sci. 109 (1981) 390.
- [11] N.R. Avery, Chem. Phys. Lett. 96 (1983) 371.
- [12] H. Steininger, S. Lehwald and H. Ibach, Surf. Sci. 123 (1982) 1.
- [13] B.A. Gurney, W. Ho, L.J. Richter and J.S. Villarrubia, Rev. Sci. Instrum. 59 (1988) 22.
- [14] L.J. Richter, W.D. Mieher, L.J. Whitman, W.A. Noonan and W. Ho, Rev. Sci. Instrum. 60 (1989) 12.
- [15] J.L. Gland, Surf. Sci. 71 (1978) 327; J.L. Gland and E.B. Kollin, Surf. Sci. 104 (1981) 478.
- [16] D. Lackey, M. Surman and D.A. King, Vacuum 33 (1983) 867.
- [17] G.B. Fisher and B.A. Sexton, Phys. Rev. Lett. 44 (1980) 683.

- [18] A.V. Melo, W.E. O'Grady, G.S. Chottiner and R.W. Hoffman, *Appl. Surf. Sci.* 21 (1985) 160.
- [19] T.A. Germer and W. Ho, *Chem. Phys. Lett.* 163 (1989) 449.
- [20] T.A. Germer and W. Ho, *J. Chem. Phys.* 93 (1990) 1474.
- [21] H. Ibach and S. Lehwald, *Surf. Sci.* 91 (1980) 187.
- [22] B.A. Sexton, *Surf. Sci.* 94 (1980) 435.
- [23] F.T. Wagner and T.E. Moylan, *Surf. Sci.* 191 (1987) 121.
- [24] G.E. Mitchell, S. Akhter and J.M. White, *Surf. Sci.* 166 (1986) 283;  
G.E. Mitchell and J.M. White, *Chem. Phys. Lett.* 135 (1987) 84.
- [25] T. Matsushima, *Surf. Sci.* 123 (1982) L663; *Surf. Sci.* 127 (1983) 403.
- [26] W.D. Miehler and W. Ho, *J. Chem. Phys.* 91 (1989) 2755.
- [27] W.D. Miehler and W. Ho, *J. Chem. Phys.* 99 (1993) 9279.
- [28] W.D. Miehler, R.A. Pelak and W. Ho, to be published.
- [29] B.A. Gurney and W. Ho, *J. Chem. Phys.* 87 (1987) 1376.
- [30] A.B. Anton and D.C. Cadogan, *Surf. Sci.* 239 (1990) L548.
- [31] B. Hellsing, B. Kasemo, S. Ljungström, A. Rosén and T. Wahnström, *Surf. Sci.* 189 (1987) 851;  
B. Hellsing and B. Kasemo, *Chem. Phys. Lett.* 148 (1988) 465;
- S. Ljungström, B. Kasemo, A. Rosén, T. Wahnström and E. Fridell, *Surf. Sci.* 216 (1989) 63;  
T. Wahnström, E. Fridell, S. Ljungström, B. Hellsing, B. Kasemo and A. Rosén, *Surf. Sci.* 223 (1989) L905.
- [32] T.M. Orlando, A.R. Burns, E.B. Stechel and D.R. Jennison, *J. Chem. Phys.* 93 (1990) 9197.
- [33] E.B.D. Bourdon, P. Das, I. Harrison, J.C. Polanyi, J. Segner, C.D. Stanners, R.J. Williams and P.A. Young, *Faraday Disc. Chem. Soc.* 82 (1986) 343;  
I. Harrison, J.C. Polanyi and P.A. Young, *J. Chem. Phys.* 89 (1988) 1498.
- [34] C.-C. Cho, J.C. Polanyi and C.D. Stanners, *J. Chem. Phys.* 90 (1989) 598.
- [35] D.V. Chakarov and W. Ho, *J. Chem. Phys.* 94 (1991) 4075.
- [36] H. Okabe, *Photochemistry of Small Molecules* (Wiley, New York, 1978).
- [37] H. Ibach and S. Lehwald, *Surf. Sci.* 76 (1978) 1.
- [38] D. Burgess, Jr., R.R. Cavanaugh and D.S. King, *Surf. Sci.* 214 (1989) 358.
- [39] C.T. Campbell, G. Ertl and J. Segner, *Surf. Sci.* 115 (1982) 309.
- [40] J.L. Gland and B.A. Sexton, *J. Catal.* 68 (1981) 286.